Buckling and Final Failure of Graphite/PEEK Stiffener Sections

Scott M. Causbie*
Boeing Commercial Airplane Company, Seattle, Washington
and
Paul A. Lagace†
Massachusetts Institute of Technology, Cambridge, Massachusetts

The buckling and final failure characteristics of midplane symmetric graphite/thermoplastic laminated angle and channel stiffener sections are investigated. Three stacking sequences with the same ply orientations, $[0_3/\pm 45]_{2s}$, $[\pm 45/0_4/\pm 45/0_2]_s$, and $[+45_2/0_6/-45_2]_s$, were chosen to model the highly directional laminates to be used in skin panel stiffeners. These laminates exhibit varying amounts of the bending-twisting coupling inherent in laminates with angle plies. The Ritz technique was employed to predict the buckling loads and modes. The experimental and analytical results for both the critical buckling load and deflection shape were in relatively good agreement. However, the accuracy of the Ritz prediction is limited by the ability to model properly the degree of elastic constraint imposed by the actual boundary conditions on the elements tested. The analysis was able to bound the actual boundary conditions. The $[+45_2/0_6/-45_2]_s$ laminate exhibited a lower buckling load than the other two laminates due to the increased bending-twisting coupling present in the laminate. This degradation was accurately predicted by the analysis. Additionally, the experimental results of the graphite/thermoplastic angle sections were compared with previously reported results for similar sections made from T300/5208 graphite/epoxy. Both the buckling and final failure characteristics of the APC-2 sections did not differ significantly from those of the sections made from T300/5208.

Nomenclature

a = element length
A = area
$\mathcal{R}_f$ = effective aspect ratio of flange
$\mathcal{R}_w$ = effective aspect ratio of web
b_f = total flange width
b_w = total web width
D_{ij} = bending matrix components (i,j = 1,2,6)
E_L = longitudinal modulus
E_T = transverse modulus
G_{LT} = shear modulus
N_{cr} = critical buckling load per length
N_x = load per length in x direction
r = radius of curvature of specimen corners
t = thickness of specimen elements
w = out-of-plane deflection
x = lengthwise direction along element
y = widthwise direction along element
Π_p = potential energy
σ_{cc} = failure stress
σ_{cr} = critical buckling stress
ν_{LT} = major Poisson's ratio

I. Introduction

In the design of modern flight vehicles, structural efficiency is a dominant criterion. Filamentary composite materials have substantially higher specific moduli and specific strengths than metals used in aerospace applications. As a result, filamentary composite materials have been used in flight vehicles to improve structural efficiency. In addition, due to the orthotropic nature of filamentary composite materials, it is possible to tailor the material to the specific design need.[1]

A common failure mode in typical flight vehicle structures is local compressive instability. Stiffened panels are one type of structure that is used in areas of flight vehicles subject to high compressive loads. Buckling is thus an important design consideration for these structures. It is necessary to understand both the initial local instabilities encountered in compressive loading of this type of structure and the behavior in the postbuckling range to final failure. Significant load-carrying capability is generally possible well into the postbuckled region. This postbuckling load-carrying capability of filamentary composite structures is an important asset that can be used to attain further weight savings. An understanding of the compressive instability of this type of structure would enable a more efficient application of filamentary composite materials.

A considerable amount of work has been conducted on the buckling of composites, and much of this has recently been summarized by Leissa.[2] However, a large portion of this work has been devoted to composite plates. More general applications require the analysis and testing of configurations employing stiffeners, such as the work accomplished by Viswanathan and Tamekuni[3] and Dickson and Biggers.[4] An extensive test program has been performed[5] on the local buckling, postbuckling, and final failure behavior of graphite/epoxy short, thin-wall compression members. Cruciform, channel, and hat section specimens were tested to model typical sections and boundary conditions found in flight vehicle compression elements.

In order to better understand the behavior of a complex structure such as a stiffened panel, it is necessary to have a knowledge of the independent behavior of each individual element and an understanding of the interaction among the elements. As a step toward a better understanding of the entire stiffened panel structure, the present work further investigates

Received March 6, 1986; revision received Jan. 25, 1988.

*Senior Engineer.
†Associate Professor of Aeronautics and Astronautics, Technology Laboratory for Advanced Composites, Department of Aeronautics and Astronautics. Member AIAA.

the local compressive instability behavior of typical stiffener sections under uniaxial compressive loading.

The great majority of work to date has been conducted on composites with relatively brittle epoxies as the matrix. Development of new composite materials is proceeding at a high rate. New constituents such as high strain-to-failure fibers and thermoplastic matrices offer the traditional advantages of filamentary composites and increased damage tolerance.[6] The material used in the current investigation is such a composite system, APC-2 graphite/thermoplastic, manufactured by ICI and employing polyetheretherketone (PEEK) as the matrix.

II. Objectives

As previously noted, a knowledge of the behavior of the elements that make up a complex structure is a necessary step in understanding the behavior of the complex structure. The main objective of the current work is to provide insight into the buckling and final failure behavior of typical stiffener sections used in stiffened panels. Two stiffener sections are examined: angles and channels. These are representative of elements of typical stiffeners used in flight vehicle structures.

Development of an analysis method to predict the initial buckling centers around a treatment of the stiffener as made up of individual plate elements. A Ritz approach is used to predict the initial buckling of the plate elements. Whereas the experimental results for final failure strengths are obtained, no purely analytical prediction for final failure is developed in the current work.

The final objective of this work is to compare the behavior of the graphite/PEEK composite system with that of typical graphite/epoxy systems. It is not anticipated that using the thermoplastic matrix will affect the initial buckling stress since using the thermoplastic does not significantly change the overall component moduli, which are the key to the initial buckling. However, the graphite/thermoplastic stiffener sections may exhibit different final failure stresses and modes than similar sections made from standard graphite/epoxy. A common failure mode of graphite/epoxy laminates loaded in compression is a local phenomenon involving buckling and delamination of individual or groups of plies.[7] The specimens made from the APC-2 system may be able to resist this local delamination problem due to their increased interlaminar fracture toughness.[8]

III. The Experiment

Test Matrix

Six different geometries of the two basic angle and channel configurations, shown in Fig. 1, were investigated. A constant specimen aspect ratio (specimen length over flange width) of 5 is maintained for all the angle section specimens. Three flange aspect ratios $\mathcal{R}_f$ were used: 9.1, 12.7, and 17.0. These were chosen so that the various specimens would exhibit varying amounts of postbuckling capability. In this context, the amount of postbuckling capability is defined as the ratio of the final failure load to the buckling load. All the channel section specimens have a specimen aspect ratio (specimen length over web width) of 3. Once again, three different web aspect ratios $\mathcal{R}_w$ of 20.9, 27.9, and 35.0 were investigated. Again, these were chosen so that the specimens exhibited varying amounts of postbuckling capability. The ratio of the flange width to the web width in all channel section specimens is 0.24.

All specimens were sized to avoid Euler column buckling and in-plane material fracture before buckling and to make the flange, in the angle section specimens, and the web, in the channel section specimens, the critical elements. Three specimens of each configuration were tested. The entire test matrix is shown in Table 1. It should be noted that the element aspect ratio takes into account the fact that part of the element width is made up of the adjoining elements and should not be considered in determining critical widths in buckling. The effective width is taken from the points halfway through the adjoining elements. Thus, the effective aspect ratios are

$$\mathcal{R}_f = [(b_f - t/2)/t] \tag{1}$$

for the flange and

$$\mathcal{R}_w = (b_w - t)/t \tag{2}$$

for the web.

Three different stacking sequences were investigated: $[0_3/\pm 45]_{2s}$, $[\pm 45/0_4/\pm 45/0_2]_s$, and $[+45_2/0_6/-45_2]_s$. All laminates are 20 plies of graphite/polyetheretherketone (PEEK) APC-2 manufactured by Imperial Chemical Industries. Although the laminates have identical in-plane properties with a longitudinal modulus of 74 GPa, their flexural properties differ due to the varied stacking sequence, as summarized in Table 2. The change in the flexural properties will affect the buckling and postbuckling behavior of the plates. Of particular importance are the D_{16} and D_{26} terms that represent the coupling between bending and twisting. These components are maximized in the $[+45_2/0_6/-45_2]_s$ laminate.

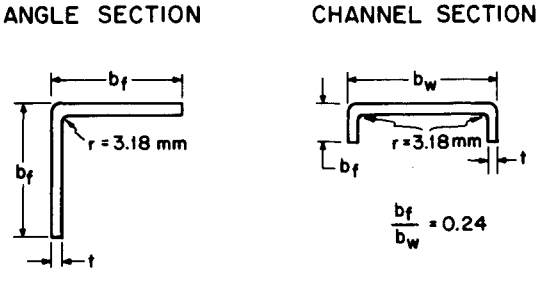

Fig. 1 Specimen cross sections.

Table 1 Test matrix and specimen[a] dimensions

Laminate	Angle sections			Channel sections				
	Length, mm	b_f, mm	$\mathcal{R}_f$	Length, mm	b_w, mm	b_f, mm	$\mathcal{R}_w$	$\mathcal{R}_f$
$[0_3/\pm 45]_{2s}$	140	27.9	9.1	191	63.5	15.2	20.9	4.8
	191	38.1	12.7	251	83.8	20.3	27.9	6.5
	254	50.8	17.0	312	104.0	25.4	35.0	8.3
$[\pm 45/0_4/\pm 45/0_2]_s$	140	27.9	9.1	191	63.5	15.2	20.9	4.8
	191	38.1	12.7	251	83.8	20.3	27.9	6.5
	254	50.8	17.0	312	104.0	25.4	35.0	8.3
$[+45_2/0_6/-45_2]_s$	140	27.9	9.1	191	63.5	15.2	20.9	4.8
	191	38.1	12.7	251	83.8	20.3	27.9	6.5
	254	50.8	17.0	312	104.0	25.4	35.0	8.3

[a]Three specimens of each configuration were tested.

Manufacture

Two 1.2 m × 1.2 m flat plates of each of the three laminate types were made. The individual plies were cut and subsequently tacked together with the use of a soldering iron. Consolidation of the laminates was achieved by autoclaving under vacuum and 0.34 MPa chamber pressure at a temperature of 372°C for 5 min. These completed plates were rough cut to smaller sections of dimensions slightly larger than the final specimen sizes. The angle and channel configurations were achieved by placing the rough-cut pieces on a heated platen covered with an insulating cloth and heated to 372°C. The laminate became sufficiently malleable to be formed and was transferred to a forming tool and pressure applied by means of a hydraulic press to form the laminate into the desired shape. The forming tools are constructed of aluminum with one tool side being solid aluminum and the other being aluminum covered with a layer of elastomeric rubber. All tool radii, and thus specimen radii, are 3.18 mm. This procedure gave consistent specimen quality. The resin content measured by an acid digestion technique was 29% compared to a nominal value of 32%. The average measured thickness of the specimens was 2.87 mm compared to a nominal value of 2.90 mm as calculated from the manufacturer's reported per ply thickness. Additionally, the coefficient of variation of the thickness measurements was less than 3%, indicating the ability to attain consistent specimen quality. Specimens were machined to final test dimensions on a diamond grit wire-cutting machine cooled by water solution. Edge quality and dimensional accuracy achieved by this process were excellent.

The specimens were prepared for testing by potting each end using an aluminum-filled potting compound (epoxy compound Epocast 33-A). Aluminum rings, 12 mm deep, were used to contain the potting compound. The potting was accomplished on a flat marble table, and 24 h elapsed before the specimen was turned over to pot the opposite end. This procedure guarantees that the two ends are parallel to the degree achieved in the machining process.

Instrumentation and Testing

Each element of each specimen is instrumented with back-to-back axial strain gages at the center of the element section. Gaging was accomplished subsequent to potting using Micro-Measurements gage CEA-060-125UW-350.

In addition to the data taken from these gages, out-of-plane deflections were measured using linearly varying deflection transducers (LVDT). For the angle section specimens, an LVDT was used on the edge of each flange directly adjacent to the strain gages. On the channel section specimens, three deflection measurements were taken along the center of the web at the quarter, half, and three-quarters points. The placement of the LVDT's and strain gages are illustrated for the two specimen types in Fig. 2.

Testing was accomplished on a Materials Test System (MTS) testing machine under stroke control at a rate of 0.76 mm/min. The specimens were placed in the testing machine with a fixed flat head at the top and a special alignment jig on the bottom. This jig allowed for slight rotation to compensate for any misalignment of the two edges. A small load is applied and then locking bolts tightened on the alignment jig. Compressive load is applied up to 10% of the expected buckling load. Strain gage readings are examined for any discrepancies in the back-to-back readings, which are corrected by adjustment of the alignment bolts in the alignment fixture. This secondary alignment procedure was generally not necessary. After this procedure, the specimens are returned to the original position and then run monotonically to failure with the strain gage and deflection data acquired automatically at the rate of 50 points/min. Failure was deemed to have occurred if the specimen was unable to carry at least 10% of the maximum load achieved.

Table 2 Bending matrix component values

Laminate	Bending matrix components, $N \cdot m$					
	D_{11}	D_{22}	D_{12}	D_{16}	D_{26}	D_{66}
$[0_3/\pm 45]_{2s}$	191	29.9	16.3	2.2	2.2	21.7
$[\pm 45/0_4/\pm 45/0_2]_s$	143	48.2	31.0	3.7	3.7	36.5
$[+45_2/0_6/-45_2]_s$	150	45.5	28.8	25.0	25.0	34.2

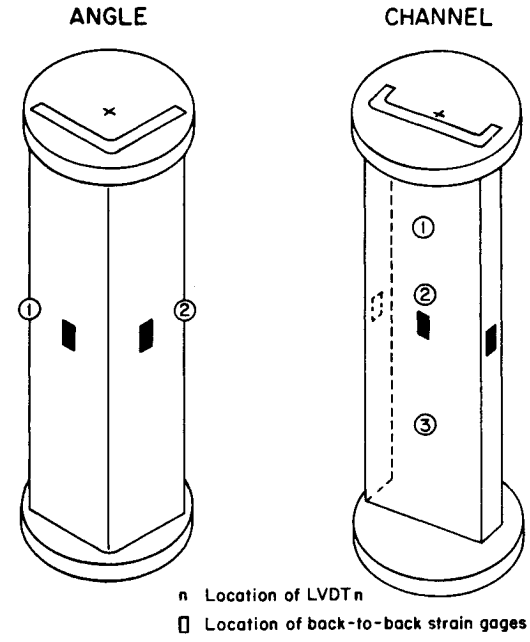

Fig. 2 Illustration of two specimen types indicating placement of instrumentation.

IV. Analytical Technique

The Ritz solution technique is employed to predict initial local buckling on an element basis. This consists of assuming deflection shapes of the buckled elements that satisfy the geometric boundary conditions. The out-of-plane deflection w shapes are substituted into the energy equation for a plate under uniaxial load N_x:

$$\Pi_p = \frac{1}{2}\iint_A \left[D_{11}\left(\frac{\partial^2 w}{\partial x^2}\right)^2 + 2D_{12}\left(\frac{\partial^2 w}{\partial x^2}\right)\left(\frac{\partial^2 w}{\partial y^2}\right) + D_{22}\left(\frac{\partial^2 w}{\partial y^2}\right)^2 + 4D_{16}\left(\frac{\partial^2 w}{\partial x^2}\right)\left(\frac{\partial^2 w}{\partial x \partial y}\right) + 4D_{26}\left(\frac{\partial^2 w}{\partial y^2}\right)\left(\frac{\partial^2 w}{\partial x \partial y}\right) + 4D_{66}\left(\frac{\partial^2 w}{\partial x \partial y}\right)^2 + N_x\left(\frac{\partial w}{\partial x}\right)^2 \right] dA \tag{3}$$

The points at which the potential energy is stationary are determined by taking partial derivatives. The eigenvalues of the resulting matrix equation are the stable equilibrium values with the lowest eigenvalue yielding the critical buckling load N_{cr}. The corresponding eigenvector corresponds to the buckled shape. An excellent discussion of this methodology as applied to laminated plates is given by Ashton and Whitney.[9]

The key to the success of this methodology is the proper selection of the deflection shapes. For the sake of efficiency, modes that expedite convergence are also desirable. In actual structures, as in the specimens investigated herein, the edge constraints are usually free or somewhere in the region between simply supported and clamped. Traditionally, the difficulty involved in accurately determining the degree of elastic constraint at a boundary that is neither fully clamped nor simply supported led to the assumption of simply supported edges, which results in a conservative prediction. Thus, the limiting cases of clamped and simply supported edges, along

with the case of free edges where applicable, are used to model and bound the behavior of the specimens. In this investigation, any edge with no support is a free edge; the loaded ends of the specimen are modeled both as simply supported and clamped in order to bound the problem, and the point at which two plate elements of a specimen (i.e., web and flange of a channel section) meet is considered simply supported. There actually is some support provided by the neighboring element, but the simply supported assumption is close to the actual condition and does provide the conservative bound.

From these considerations, four sets of deflection shapes were assumed for the four different combinations of boundary conditions. These are summarized in the Appendix. Special attention was given to use modes that will allow for the effects of bending-twisting coupling. The number of terms taken in the assumed series was determined by convergence studies. It is important to note that these are specifically applicable to the laminates investigated with their corresponding amounts of bending-twisting coupling and their aspect ratios. More terms may be required for laminates with greater amounts of such coupling or higher aspect ratios.

As a means of checking the accuracy of this analysis, the program was run for cases with no bending-twisting coupling so as to compare these results with the exact solutions available for these specially orthotropic laminates. In all these cases, the current methodology yielded buckling loads within 1% of the exact solution. It should be noted that transverse shear effects were not included in the current analysis. Inclusion of such effects would yield a more accurate solution.

V. Results

Stress-Strain and Initial Buckling

Back-to-back strain gage readings for the specimens follow a pattern of initially diverging gradually as load increases and then diverging drastically as local buckling of the gaged element occurs, as shown in Fig. 3. The longitudinal moduli for each specimen were determined by performing a least-squares fit on the linear region of the back-to-back strain vs stress plots. These results are reported in Table 3. The average measured value of 72.1 GPa is very close to the predicted value of 74 GPa. This value is derived using classical laminated plate theory and the values for the elastic constants of a basic unidirectional APC-2 ply listed in Table 4. Plots of stress vs out-of-plane deflection also show the large increase of deflection associated with the buckling of the element, as seen in Fig. 4.

Southwell plots were used to determine the experimental buckling loads. Southwell plots are generated by plotting load divided by out-of-plane deflection, measured via the LVDT, vs the out-of-plane deflection. A linear regression is performed to determine the buckling load. The experimental buckling stresses σ_{cr} determined in this manner are also reported in Table 3, along with the predictions using the Ritz technique. Two predictions were made for each specimen configuration, assuming clamped and then simply supported conditions for the loaded edges. It should be noted that the channel specimens with the lowest aspect ratio $\mathcal{R}_w = 20.9$ did not buckle prior to final failure.

The two predicted buckling stresses do indeed bound the experimental values for the angle section specimens. However, this does not occur for the channel section specimens that exhibit buckling stresses slightly higher than the predictions assuming clamped loaded edges. This conservative prediction is attributed to the assumption that the edges of the web are simply supported. The unbuckled flanges of the channel section actually provide a greater constraint on the web. Further analyses should be performed to better bound this behavior.

A comparison of the three deflection readings along the longitudinal directions of the webs of the channel specimens gives a good indication of the buckled shape of the web. Investigation of these deflection readings just following buckling shows that the webs of the channels generally buckled in one full sine wave, shifted slightly in the $[+45_2/0_6/-45_2]_s$ laminate in which a large amount of bending-twisting coupling is present. The angle section specimens always buckled in a one-half sine wave pattern typical of specimens with one free edge. Three-dimensional plots of the predicted buckled shapes show that the deflection shapes predicted by the Ritz method are similar to those observed experimentally.

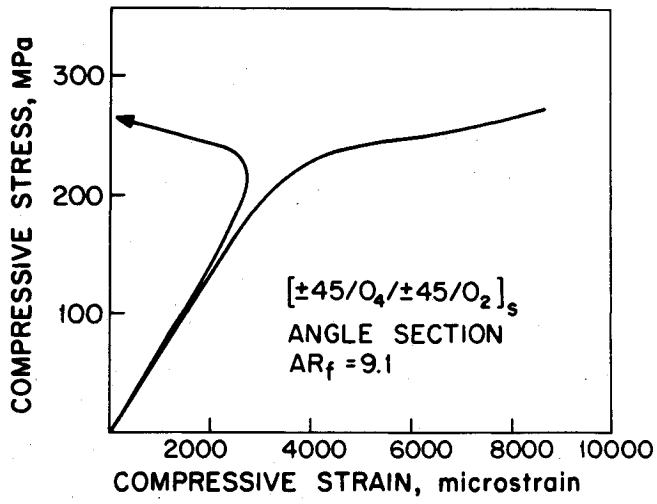

Fig. 3 Typical stress vs strain plot for angle section specimens.

Table 3 Longitudinal moduli and buckling stresses

	Angle sections					Channel sections				
				Predicted σ_{cr}, MPa					Predicted σ_{cr}, MPa	
Laminate	$\mathcal{R}_f$	E_L, GPa	σ_{cr}, MPa	SS[a]	Clamped[b]	$\mathcal{R}_w$	E_L, GPa	σ_{cr}, MPa	SS[a]	Clamped[b]
$[0_3/\pm 45]_{2s}$	9.1	74.1 (8.9%)[c]	213 (4.8%)	159	258	20.9	68.0 (1.5%)	[d]	249	311
	12.7	74.9 (3.9%)	113 (4.2%)	84	137	27.9	72.8 (5.3%)	187 (5.4%)	139	176
	17.0	68.0 (6.3%)	69 (1.5%)	47	76	35.0	71.4 (4.1%)	130 (8.9%)	90	113
$[\pm 45/0_4/\pm 45/0_2]_s$	9.1	72.1 (6.1%)	258 (6.0%)	237	309	20.9	64.6 (3.3%)	[d]	356	387
	12.7	77.6 (3.7%)	143 (3.4%)	124	164	27.9	71.4 (2.0%)	236 (4.0%)	199	218
	17.0	73.5 (4.5%)	82 (2.8%)	69	91	35.0	74.2 (4.9%)	157 (2.7%)	126	139
$[+45_2/0_6/-45_2]_s$	9.1	68.0 (6.2%)	166 (6.0%)	167	228	20.9	74.2 (2.0%)	[d]	292	320
	12.7	72.1 (1.2%)	98 (1.1%)	88	176	27.9	71.4 (0.4%)	179 (0.3%)	164	179
	17.0	79.0 (4.9%)	61 (1.5%)	49	61	48.8	70.8 (1.5%)	124 (4.7%)	104	115

[a]Loaded edges assumed simply supported.
[b]Loaded edges assumed clamped.
[c]Numbers in parentheses are coefficients of variation.
[d]Specimens did not buckle before failure.

Close examination of Table 3 results in three major observations concerning the buckling loads. First, the buckling loads of the channel section specimens always exceed those of the angle section specimens, although the channel sections have higher aspect ratios. This is expected because the critical element in the channel section, the web, is supported on two sides by flanges, whereas the critical flange in the angle is only supported on one side. Second, as expected, the buckling load decreases as the critical element aspect ratio increases. This trend was properly modeled by the analytical technique. The third observation involves the laminate stacking sequence. For both the angle and channel section specimens, the $[\pm 45/0_4/\pm 45/0_2]_s$ laminate had the highest buckling stress for any particular geometry, while the $[+45_2/0_6/-45_2]_s$ laminate always had the lowest buckling stress. This trend was also predicted by the Ritz technique and is a consequence of the value of the bending stiffnesses that were summarized in Table 2. The superiority of the $[\pm 45/0_4/\pm 45/0_2]_s$ configuration is due to this laminate possessing the highest value of the D_{66} component. On the other hand, despite having a high D_{66} component, the $[+45_2/0_6/-45_2]_s$ laminate has very large coupling terms D_{16} and D_{26}, which causes the observed degradation in buckling load.

Postbuckling and Final Failure

Behavior in the postbuckling range was characterized by sharp divergence of the back-to-back strain gages and large increases in the out-of-plane deflections, as may be seen in Figs. 3 and 4. Buckling of the adjacent element(s) occurs almost immediately after the buckling of the critical element. Abrupt drops in the load-carrying capability of the specimens sometimes occurred in the postbuckling region, indicating damage to the specimen has occurred in the form of delamination and failure of the individual plies, as observed. As both types of specimens have free edges, it is likely that delamination originated at these edges. In many cases where delamination was observed, it was observed at such an edge.

As previously noted, failure was deemed to have occurred if the specimen could no longer carry at least 10% of the maximum attained load. The failure stresses σ_{cc} are defined as the maximum attained stresses and are presented in Table 5, along with the ratio of the failure stress to the buckling stress. This latter parameter indicates the amount of postbuckling load-carrying capability of the specimen. However, the failure of the channel section specimens generally occurred in the flanges and, thus, the final failure of these specimens is not a true indication of the postbuckling capability of the web.

In general, the same trends were followed by the failure stresses of the specimens as for the buckling stresses of the specimens: the stresses decrease with increasing aspect ratio, and the $[\pm 45/0_4/\pm 45/0_2]_s$ laminate had the highest failure stresses, with the $[+45_2/0_6/-45_2]_s$ laminate having the lowest. However, the angle section specimens generally failed at the same or slightly higher stresses than similarly sized channel specimens. This is because the failure in the channel sections occurred in the flanges and, thus, was not a true measure of the capability of the web to carry load. Furthermore, it is interesting to note that the parameter that expresses the final failure stress divided by the buckling stress is relatively independent of laminate configuration for a given specimen geometry. This may be attributed to the very local nature of the damage leading to final failure as subsequently described.

Examination of the failed specimens shows that the dominant failure mode is a combination of ply buckling, delamination of the outer plies, and severe separation of groups of plies of the laminate. These characteristics may be seen in the photograph of a failed specimen in Fig. 5. The ply buckling and delamination is characterized by the outer one of two plies buckling off and the failure occurring directly under this region. This is very similar to the behavior described by Vizzini and Lagace[7] in their work on the compressive failure of composite tubes.

Table 4 Basic ply compressive elastic properties

Material property	Material system	
	APC-2	T300/5208
E_{11}	110 GPa	131 GPa
E_{22}	8.2 GPa	10.5 GPa
G_{12}	5.5 GPa	7.17 GPa
ν_{12}	0.34	0.33

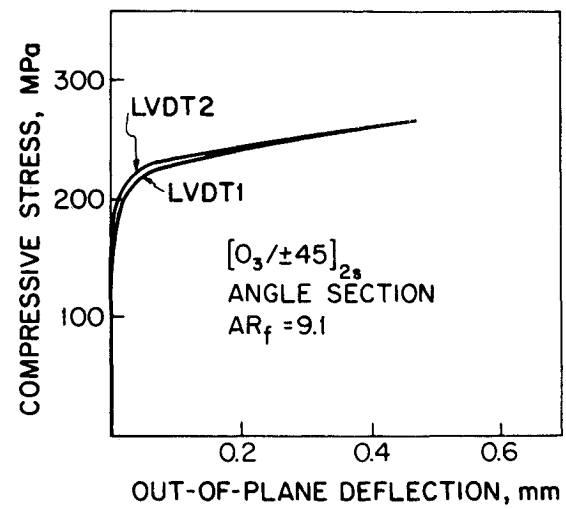

Fig. 4 Typical stress vs out-of-plane deflection plot for angle section specimens.

Table 5 Failure stresses and postbuckling ratios

Laminate	Angle sections			Channel sections		
	AR_f	σ_{cc}, MPa	σ_{cc}/σ_{cr}	AR_w	σ_{cc}, MPa	σ_{cc}/σ_{cr}
$[0_3/\pm 45]_{2s}$	9.1	311[a]	1.46	20.9	273 (5.8%)	[b]
	12.7	238 (3.0%)[c]	2.10	27.9	221 (2.4%)	1.18
	17.0	187[a]	2.71	35.0	196 (4.0%)	1.51
$[\pm 45/0_4/\pm 45/0_2]_s$	9.1	322 (5.7%)	1.25	20.9	322 (4.8%)	[b]
	12.7	264 (4.1%)	1.85	27.9	251 (1.0%)	1.06
	17.0	205 (7.5%)	2.51	35.0	228 (3.5%)	1.45
$[+45_2/0_6/-45_2]_s$	9.1	228 (1.3%)	1.37	20.9	288 (1.4%)	[b]
	12.7	193 (3.3%)	1.97	27.9	229 (1.3%)	1.28
	17.0	152 (2.6%)	2.51	35.0	195 (2.5%)	1.57

[a]Two of three specimens failed at ends and are not reported.
[b]Specimens did not buckle before failure.
[c]Numbers in parentheses are coefficients of variation.

There was virtually no deviation in the failure mechanisms for the different laminates and geometrical configurations. The laminates with the 45 deg plies on the outer surface exhibited this ply buckling to the greatest degree. But this behavior was observed in all laminates tested in the current work. The large scale ply separation of the laminates generally occurred in the innermost plies of the laminate, in effect tearing the laminate in half.

VI. Comparison of APC-2 and T300/5208

The behavior of the APC-2 angle sections determined herein is compared in Figs. 6 and 7 to results for similar sections made from T300/5208[10] in terms of the critical buckling stresses and the final failure stresses vs element aspect ratio. The tests of the specimens made from T300/5208 graphite/epoxy were conducted on specimens with similar geometry but with a layup $[\pm 45/0_4]_{2s}$ that was different from any of the specimens investigated herein. However, comparisons can still be made, despite these differences, with the current laminate that most closely corresponds to this stacking sequence: $[\pm 45/0_4/\pm 45/0_2]_s$. It must also be noted that the graphite/epoxy specimens are 24 plies amounting to a thickness of 3.40 mm, whereas the graphite/thermoplastic specimens are 20 plies measuring 2.89 mm. The elastic constants of the two systems are shown in Table 4.

Nevertheless, the comparisons are striking in that there is no appreciable difference in the behavior of the specimens made from the two material systems, both in terms of the buckling stress and the failure stress. Some slight differences in buckling stresses would be expected due to the slight differences in geometry. But the comparison of results does indicate that the graphite/PEEK system is just as capable as the graphite/epoxy system in terms of buckling. This further implies that buckling work done on graphite/epoxy systems is applicable to the newer graphite/thermoplastic systems.

On the other hand, the anticipated advantages of the thermoplastic matrix in preventing delamination did not materialize for this loading situation. The failure in both cases is controlled by local ply buckling and delamination, and it was hoped that the increased resistance to delamination of the thermoplastic, as reported in interlaminar fracture toughness tests,[8] would yield an increased ability to carry load in the postbuckling range. However, the results indicate that, considering the thickness difference, the graphite/thermoplastic system behaves only slightly better than the graphite/epoxy system. Nevertheless, the graphite/PEEK system is still at least as useful as the graphite/epoxy system in carrying load in this situation.

VII. Summary

The buckling and final failure characteristics of graphite/thermoplastic angle and channel section stiffeners were investigated experimentally and with the use of a Ritz analysis. Both the analytical and experimental results indicate that buckling load decreases as 1) the side boundary conditions of the critical stiffener element become less restrictive, 2) the aspect ratio (effective width/thickness) of the critical stiffener element is increased, 3) the D_{66} bending stiffness term decreases, and 4) the bending-twisting coupling terms D_{16} and D_{26} increase. The Ritz analysis was able to bound the observed buckling loads of the $[0_3/\pm 45]_{2s}$, $[\pm 45/0_4/\pm 45/0_2]_s$, and $[+45_2/0_6/-45_2]_s$ angle section specimens, but the inability to

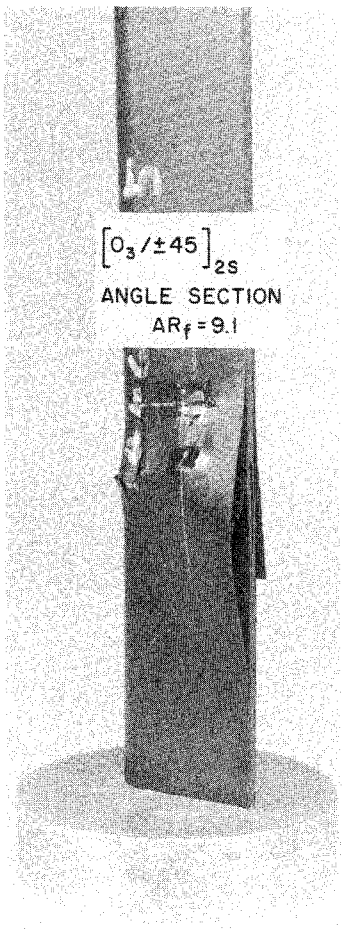

Fig. 5 Photograph of failure of $[0_3/\pm 45]_{2s}$ angle section specimen illustrating ply buckling and delamination.

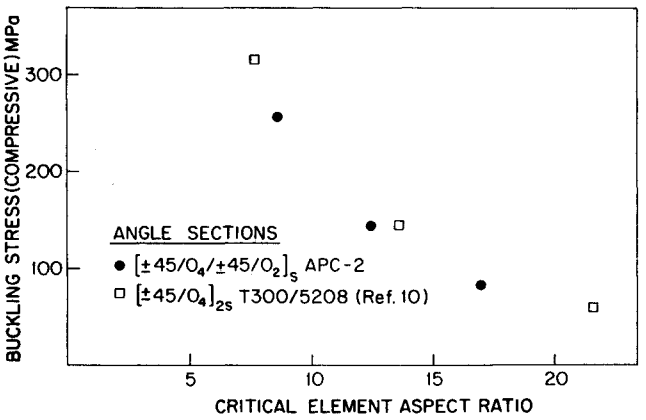

Fig. 6 Buckling stress vs critical element aspect ratio for angle section specimens.

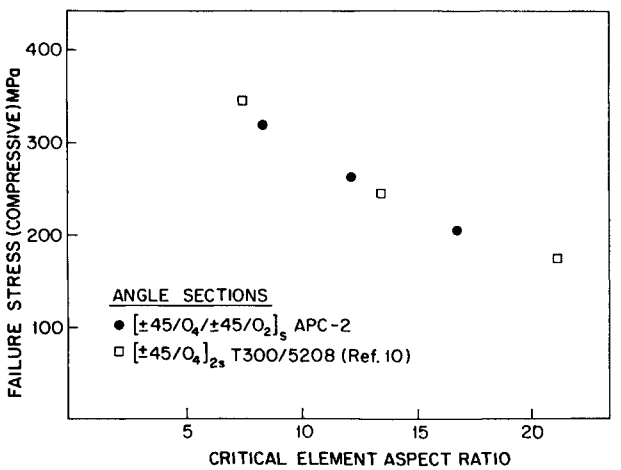

Fig. 7 Failure stress vs critical element aspect ratio for angle section specimens.

model precisely the actual degree of elastic constraint of the element edges where they meet adjoining elements caused the predictions to be slightly conservative for the channel sections. Further work is needed to better quantify these effects.

The final failure of all specimens was characterized by local ply buckling and delamination followed by more extensive delamination of several plies. The ultimate load-carrying capability of the specimens approximately followed the same trends as the buckling stresses. However, the postbuckling capacity, as defined by the failure stress divided by the buckling stress, was relatively independent of the stacking sequence. This may be attributable to the local nature of the damage causing final failure. Furthermore, final failure of the channel specimens occurred in the flanges, thus not providing a true test of the ultimate load-carrying capacity of the web. Further tests should be conducted with different geometries to prompt final failure in the web.

Comparison of the results for the graphite/thermoplastic angle sections determined herein with similar graphite/epoxy results show that there is no appreciable difference in the behavior, both in terms of buckling and failure stresses. This implies that the APC-2 system is just as capable as the traditional graphite/epoxy system in buckling but also that the reported increased resistance to delamination of the APC-2 did not inhibit the local delamination failure mode and was thus unable to cause an increase in the ultimate load-carrying capability of the stiffeners.

Appendix

The assumed series for the out-of-plane deflection w used in the Ritz analysis for the four boundary conditions are:

1) Simply supported on loaded ends and sides (channel section web):

$$w = \sum_{m=1}^{6} \sum_{n=1}^{2} A_{mn} \sin\left(\frac{m\pi x}{a}\right) \sin\left(\frac{n\pi y}{b}\right) \tag{A1}$$

2) Simply supported on loaded ends; simply supported on one side; free on other side (flange):

$$w = \sum_{m=1}^{3} \sum_{n=1}^{3} \sum_{p=1}^{3} \sin\left(\frac{m\pi x}{a}\right) \left[A_{mn} \sinh\left(\frac{ny}{b}\right) + B_{mp} \sin\left(\frac{p\pi y}{b}\right)\right] \tag{A2}$$

3) Clamped on loaded ends; simply supported on sides (channel section web):

$$w = \sum_{n=1}^{6} \sum_{m=1}^{2} A_{mn} \left\{\cos\left[\frac{(m+1)\pi x}{a}\right] - \cos\left[\frac{(m-1)\pi x}{a}\right]\right\} \sin\left(\frac{n\pi y}{b}\right) \tag{A3}$$

4) Clamped on loaded ends; simply supported on one side; free on other side (flange):

$$w = \sum_{n=1}^{5} \sum_{m=1}^{3} \sum_{p=1}^{3} \left\{\cos\left[\frac{(m+1)\pi x}{a}\right] - \cos\left[\frac{(m-1)\pi x}{a}\right]\right\} \times \left[A_{mn} \sinh\left(\frac{ny}{b}\right) + B_{mp} \sin\left(\frac{p\pi y}{b}\right)\right] \tag{A4}$$

Acknowledgments

This work was performed while the first author was a graduate student working at the Boeing Military Airplane Company in Wichita, Kansas, under the auspices of the Engineering Internship Program of the Massachusetts Institute of Technology. This author would like to gratefully acknowledge the help of Don Fusco and Richard Grubb in the computer implementation of the analysis.

References

[1]Dastin, S., Eidinoff, H. C., and Arman, H., Jr., "Some Engineering Aspects of the X-29 Airplane," *Proceedings of the 29th National SAMPE Symposium,* Society for the Advancement of Material and Process Engineering, Covina, CA, April 1984, pp. 1438–1449.

[2]Leissa, A. W., "Buckling of Composite Plates," *Composite Structures,* Vol. 1, 1983, pp. 51–66.

[3]Viswanathan, A. V. and Tamekuni, M., "Elastic Buckling Analysis for Composite Stiffened Panels and Other Structures Subjected to Biaxial Inplane Loads," NASA CR-2216, Sept. 1973.

[4]Dickson, J. N. and Biggers, S. B., "Design and Analysis of a Stiffened Composite Fuselage Panel," NASA CR-159302, Aug. 1980.

[5]Reneiri, M. P. and Garrett, R. A., McDonnell Douglas Corp., St. Louis, MO, Rept. MDC-A7091.

[6]Willats, D. J., "Advances in the Use of High Performance Continuous Fibre Reinforced Thermoplastics," *SAMPE Journal,* Vol. 24, No. 5, Sept.-Oct. 1984, pp. 6–10.

[7]Vizzini, A. J. and Lagace, P. A., "The Role of Ply Buckling in the Compressive Failure of Graphite/Epoxy Tubes," *AIAA Journal,* Vol. 23, Nov. 1985, pp. 1791–1797.

[8]Leach, D. C., Curtis, D. C., and Tamblin, D. R., "Delamination Behavior of Carbon Fiber/Polyetheretherketone (PEEK) Composites," *Toughened Composites,* American Society for Testing and Materials, Philadelphia, PA, ASTM STP 937, 1987, pp. 358–380.

[9]Ashton, J. E. and Whitney, J. M., *Theory of Laminated Plates,* Technomic Publishing, Westport, CT, 1970.

[10]Boeing Co. Buckling Research, Boeing Co., Seattle, WA, unpublished.